

# A study of the process and kinetics of electrochemical deposition and the hydrothermal synthesis of hydroxyapatite coatings

LI-YE HUANG<sup>1,2</sup>, KE-WEI XU<sup>1</sup>, JIAN LU<sup>2</sup>

<sup>1</sup>State Key Laboratory for Mechanical Behavior of Materials, Xi'an Jiaotong University, Xi'an, 710049, P.R. China

E-mail: kwxu@xjtu.edu.cn

<sup>2</sup>LASMIS (Laboratoire des Systèmes Mécaniques et d'Ingénierie Simultanée), Université de Technologie de Troyes, 12 rue Marie Curie, BP 2060 10010, Troyes, France

E-mail: lu@univ-troyes.fr

Hydroxyapatite (HAp) coatings were prepared using electrochemical deposition and post-hydrothermal synthesis. The composition and morphology of coatings at each processing step was studied through the application of scanning electron microscopy (SEM), X-ray diffraction (XRD) and infra-red spectroscopy (IR). The mechanism and kinetics of hydrothermal synthesis were considered in particular, and the influence of the temperature and time on the HAp formation rate was also investigated. The results show that the electrochemical deposition coatings are composed of  $\text{CaHPO}_4 \cdot 2\text{H}_2\text{O}$  crystals which are converted into needle-like HAp crystals after post-hydrothermal treatment. The HAp content of the coatings increases with the treatment temperature and time. The synthesis rate also increases with the pH value of the water. The formation of HAp coatings is considered to be a combination of several reactions. An Arrhenius relationship was found between the HAp formation rate and the temperature, and an apparent activation energy of 94.4 KJ/mol was obtained by calculation.

© 2000 Kluwer Academic Publishers

## 1. Introduction

Hydroxyapatite (HAp), or  $\text{Ca}_{10}(\text{PO}_4)_6(\text{OH})_2$ , has been widely used as an implant material for many years due to its close similarity in chemical composition and high biocompatibility with natural bone tissue [1, 2]. A significant difference between HAp and biocompatible surgical metal alloys such as Ti-6Al-4V lies in the ability of HAp to form a strong chemical bond with natural bone [3]. Owing to the inferior mechanical properties of bulk HAp, such as brittleness, low tensile strength and difficulties in fabrication, significant research activities have been associated with the development of HAp coatings. Much effort has been made in recent years to develop processing technologies to coat HAp onto metallic substrate surfaces. Many technologies (such as plasma-spraying, electrophoretic deposition, sol-gel, pulse laser melting and physical vapor deposition) have been used, although disadvantages still exist in certain cases (see a detailed description in [4]). These technologies, along with their post-treatment to enhance the bond strength between the coatings and substrate, involve processing at high temperatures which can sometimes result in the decomposition of HAp. For instance, plasma-spraying is the most widely used process for fabricating HAp coatings in the implant industry, but due to the extremely

high temperature required, the coatings may contain tri- and tetra-calcium phosphate, oxyhydroxyapatite and amorphous calcium phosphates [5]. Pure HAp coatings are necessary for medical implant because other phases and constituents could accelerate the degradation of HAp coatings in the human body. In addition, it is a line-of-sight process that can produce non-uniform coatings when applied to components with complex shapes.

Some researchers [6–9] have suggested using an electrochemical deposition method to fabricate calcium phosphate coatings using aqueous electrolytes that contain Ca- and P-bearing ions. This method was claimed to have many advantages such as the possibility to obtain stoichiometric composition, high purity to a degree is not easily achieved using other processes and forming uniform coatings on bodies of complex shape, and the fact that the microstructure is a metal fiber networks [10]. The process behind this method is worth investigating for reliable application in the biomedical field.

The purpose of this study is to contribute to the understanding of how to use electrochemical deposition and post-hydrothermal treatment to prepare HAp coatings. Much attention was paid to hydrothermal treatment since HAp crystals did not appear to form if only electrochemical deposition was used. The influence of

temperature and time on the composition and morphology of the coatings was studied in detail in order to understand the kinetics of HAp formation. The Arrhenius relationship with given parameters for HAp formation was obtained by calculation.

## 2. Experimental procedure

Ti-6Al-4V alloy specimens were mechanically ground and subsequently blasted with SiC grit, rinsed with acetone in an ultrasonic bath, washed with distilled water and then used as substrates for electrochemical deposition. The electrolytes used for preparing coatings were made by mixing 0.168 M  $\text{Ca}(\text{NO}_3)_2 \cdot 4\text{H}_2\text{O}$  and 0.1 M  $\text{NH}_4\text{H}_2\text{PO}_4$ . The solutions were prepared with analytical reagents and deionized water. The pH value of the electrolytes was measured at room temperature and adjusted by ammonia.

The electrochemical deposition was performed at various voltages ranging from 1.0 to 10 V. The depositing time varied from 1 to 3 h, and the temperature from 25 to 65 °C. The Ti-6Al-4V substrates were used for the cathode and the anode consisted of two graphic rods.

The coatings prepared by electrochemical deposition were then hydrothermally treated in an autoclave. The hydrothermal treatment process was studied at various steam temperatures and pH values as shown in Table I (the treatment time was kept constant at 8 h in most cases).

Experiments for the kinetic analysis of the conversion of  $\text{CaHPO}_4 \cdot 2\text{H}_2\text{O}$  to HAp were carried out at 110, 130 and 150 °C and a treatment time of 2, 4, 6, 8 and 10 h, respectively. The pH value of the water used for the hydrothermal treatment was kept at 10 to 11.

The phase composition of the coatings was quantitatively identified by X-ray diffraction (XRD) and infrared spectroscopy (IR). The morphology and structure of the coatings were observed by scanning electron microscopy (SEM).

## 3. Results and discussion

### 3.1. XRD analysis and SEM observation

The results obtained by XRD (Fig. 1a) indicate that the electrochemical deposited coatings, prepared at 60 °C, 2.0 V and 2.5 h, contain extremely pure calcium hydrogen phosphate dihydrates ( $\text{CaHPO}_4 \cdot 2\text{H}_2\text{O}$ ). Coatings produced under these conditions are uniform and adherent, with a thickness of about 50 μm. The shape of  $\text{CaHPO}_4 \cdot 2\text{H}_2\text{O}$  crystals is plate-like (Fig. 1b). It was found that although the electrochemical deposition parameters differ, the coatings always consist of

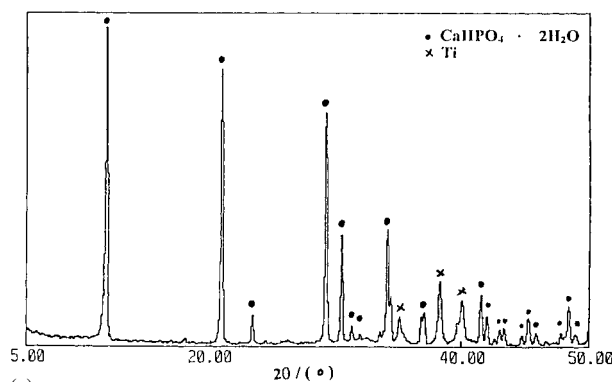


Figure 1 XRD spectra (a) and SEM photograph (b) of electrochemical deposition coating.

$\text{CaHPO}_4 \cdot 2\text{H}_2\text{O}$ . It is only the porosity and crystal size that are changed by the different parameters.

The  $\text{CaHPO}_4 \cdot 2\text{H}_2\text{O}$  turns to HAp during the post-hydrothermal treatment was demonstrated by the XRD readings (Fig. 2). Also, the HAp content of the coatings gradually increases with temperature, no matter what the pH value within a range of 7 to 11 (Fig. 3). The only difference is that when the pH value is kept at 7 and the coatings are treated for 8 h, there is nearly no detectable conversion from  $\text{CaHPO}_4$  to HAp at 120 °C (Fig. 2, No. 1). When the temperature is increased to 150 °C, HAp can be found in the coatings, with a percentage in terms of volume of 47% (Fig. 3). The HAp content increases to 78% at 180 °C. At 200 °C, the coatings consist entirely of HAp. The diffraction pattern of the coatings treated at 200 °C (Fig. 2, No. 4) matches the JCPDS X-ray Standard, with major HAp peaks corresponding to (002), (102), (210), (211), (112), (300) and (202) [11]. It was noted that at 180 °C, the relative X-ray intensity of the (300) to the (211) plane is larger than unity, quite

TABLE I The main hydrothermal treatment parameters

Samples	No. 1	No. 2	No. 3	No. 4	No. 5	No. 6	No. 7
Temperature/°C	120	150	180	200	110	130	150
pH value	7	7	7	7	10–11	10–11	10–11

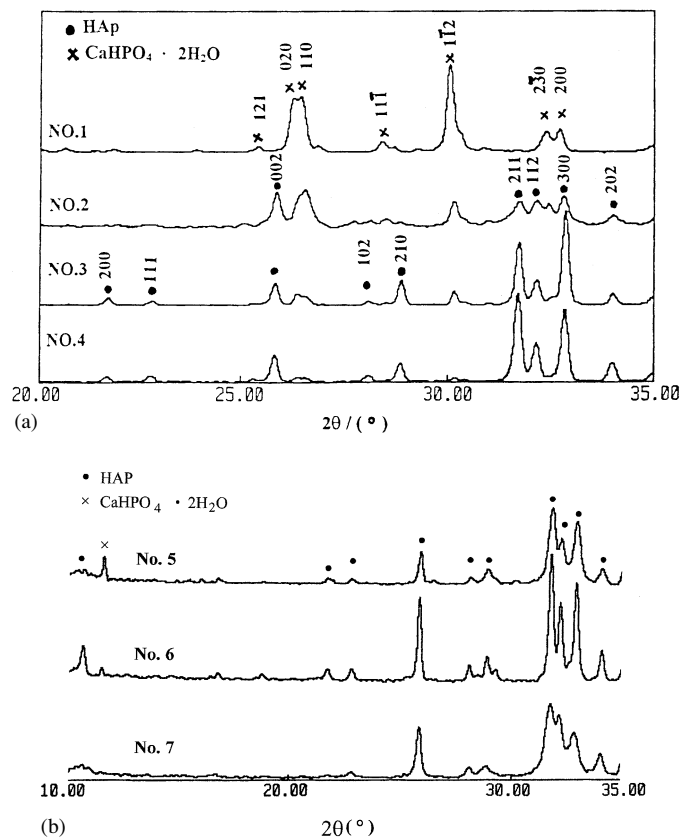


Figure 2 XRD spectra of coatings hydrothermally treated under different conditions. (a) pH = 7, (b) pH = 10–11.

different from what happens at 200 °C. This may possibly be related to preferential growth of the (300) plane below 200 °C.

Another interesting phenomenon is that the increase of the pH value causes a considerable rise in the hydrothermal reaction rate Figs 2b and 3. When the pH value increases from 7 to 10–11, the critical temperature for the formation of total HAp drops from 200 °C to 150 °C during the same treatment time (Fig. 2b, No. 7). In addition, Fig. 2b shows that the relative intensity of the (300) to (200) plane is invariably less than unity.

Fig. 4 shows the microstructure of the coatings. After post-hydrothermal treatment at 180 °C, the coatings consist of needle-like and plate-like crystals (Fig. 4a).

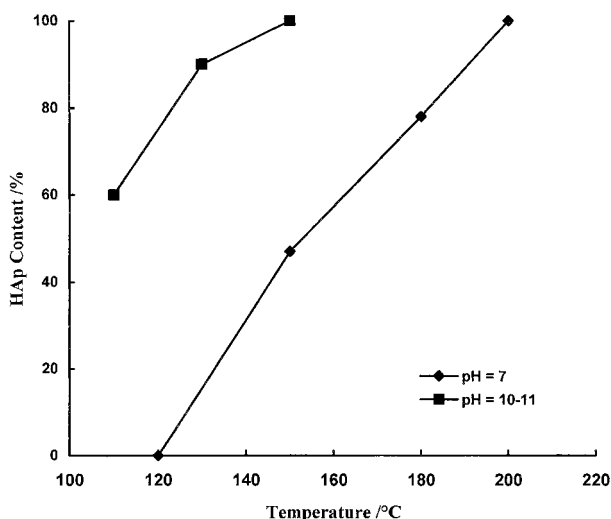


Figure 3 The content of HAp as a function of the hydrothermal treatment temperature.

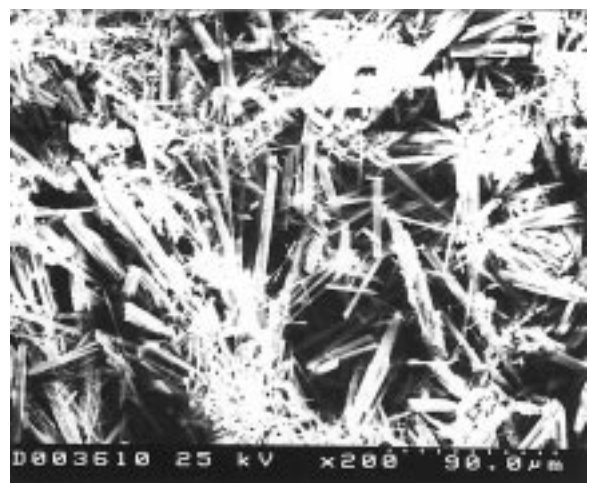
EDAX was used to measure the Ca/P mol ratio of different kinds of crystals, giving readings of 1.63 and 1.0 respectively for the needle-like and plate-like phases. By comparing these to the XRD results (Fig. 2a), it can be proved that the needle-like phases correspond to HAp, and the plate-like phases to CaHPO<sub>4</sub>. For coatings treated at 200 °C, SEM (Fig. 4b) shows an interlocking network of non-oriented needle-like crystals, which are similar in shape to the thin needle-like crystals of apatite in bone [12]. Fig. 4c shows the structure of the coatings treated at 150 °C with a pH value of 10–11. There are many plate-like particles together with a few prism-shape crystals. At a relatively high magnification (Fig. 4d), it could be seen that the plate-like particles consist of spherical aggregates formed by thin prism crystals. This suggests that the addition of ammonia might be more effective in stimulating the crystallographic growth of HAp. All of the coatings examined by SEM contain a number of pores on the surface. This is no doubt beneficial to the growth of bone tissue [13].

### 3.2. IR spectroscopic analysis

The IR transmission spectra (Fig. 5) of the coatings were obtained from KBr pellets containing fine powders removed from flat titanium alloy substrates. The IR spectrum in Fig. 5a No. 1 indicates that the coatings treated at 120 °C contain HPO<sub>4</sub><sup>2-</sup>, H<sub>2</sub>O, OH<sup>-</sup> and PO<sub>4</sub><sup>3-</sup>. The peak at 3572 cm<sup>-1</sup> is due to the stretching mode of hydroxy in HAp crystals. The 872 cm<sup>-1</sup> peak is apparently caused by HPO<sub>4</sub><sup>2-</sup> ions. The broad bands in the 3600 to 2500 cm<sup>-1</sup> range and the peak around 1648 cm<sup>-1</sup> correspond to water. The other peaks at 602, 865 and 1100–1033 cm<sup>-1</sup> are due to PO<sub>4</sub><sup>3-</sup> ions.



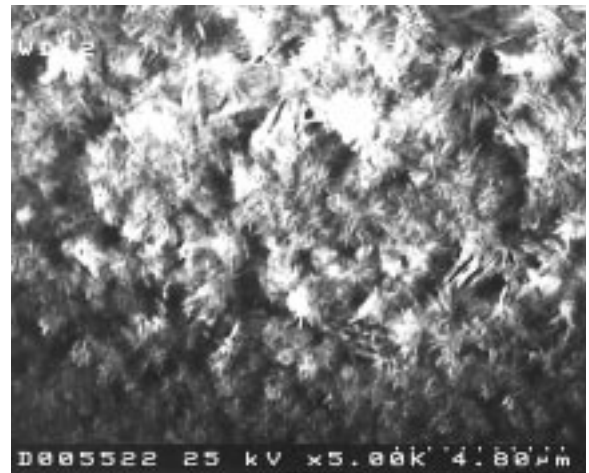
(a)



(b)



(c)

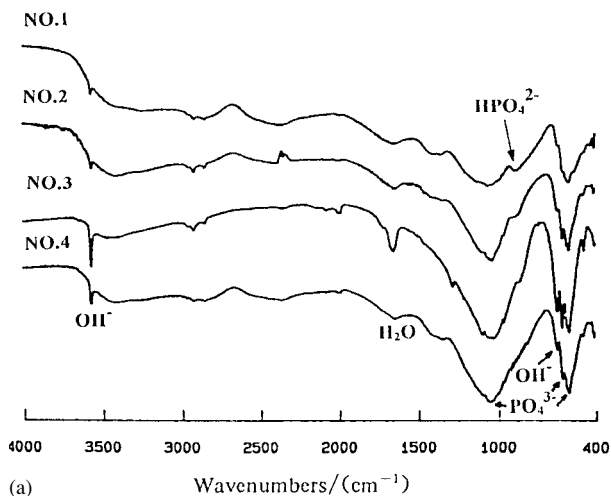


(d)

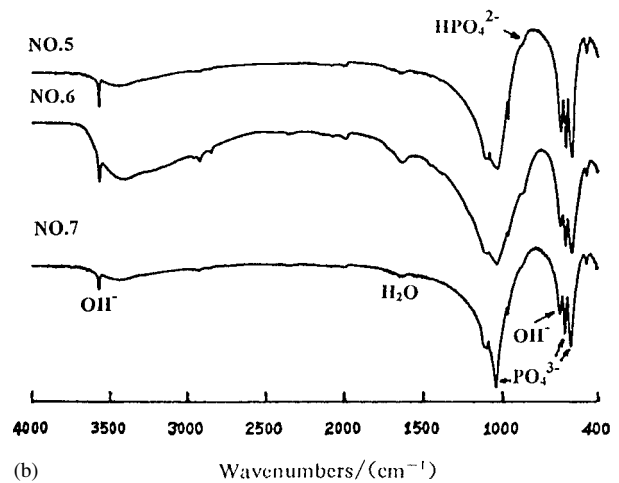
Figure 4 SEM photographs of coatings treated under different conditions: (a) pH = 7 180 °C, (b) pH = 7 200 °C, (c) and (d) pH = 10–11 150 °C.

It is worth pointing out that the characteristic peak resulting from the librational mode of hydroxy in HAP does not appear at  $634\text{ cm}^{-1}$  in Fig. 5a No. 1 [14]. This indicates that the coatings consist entirely of  $\text{CaHPO}_4$  crystals. It can be seen from Fig. 5a, Nos. 2 to 4, that as the temperature rises, the amount of  $\text{HPO}_4^{2-}$  decreases and the  $\text{HO}^-$  intensity at  $634\text{ cm}^{-1}$  increases. When the coatings are hydrothermally treated at  $200\text{ °C}$ , the

$872\text{ cm}^{-1}$  peak disappears and the  $634\text{ cm}^{-1}$  peak becomes very acute. This is very similar to what has been found both for bulk HAP of highly purity and real bone tissue [15, 16]. Fig. 5b gives the IR spectra of coatings treated hydrothermally at a higher pH value. It is clear that both the pH value and the temperature have a similar effect on the formation of HAP, which means that the IR and XRD results are in agreement.



(a)



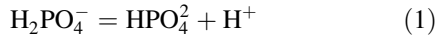
(b)

Figure 5 IR spectra of coatings treated hydrothermally under different conditions. (a) pH = 7, (b) pH = 10–11.

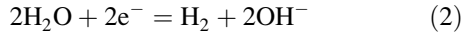
### 3.3. Analysis of the reaction mechanism

Based on the HAp formation process and the opinion of many researchers [17], the reaction progress may be a combination of several chemical reactions.

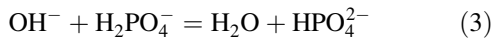
First, the electrolyte should have an equilibrium reaction:



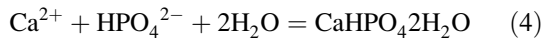
The amount of  $\text{HPO}_4^{2-}$  ions in the solution is small since the ionization constant in Equation 1 is only  $6.3 \times 10^{-8}$ . With the aid of the electric field, the water at the cathode (substrate) surface is decomposed into hydrogen gas and hydroxide ions:



Undoubtedly, the formation of  $\text{OH}^-$  can enhance the reaction in Equation 1 to produce  $\text{HPO}_4^{2-}$ . Also the  $\text{OH}^-$  may react with the  $\text{H}_2\text{PO}_4^-$  according to the equilibrium reaction below:

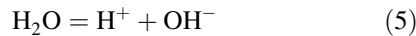


Finally, the product,  $\text{HPO}_4^{2-}$ , combines with  $\text{Ca}^{2+}$  to produce a  $\text{CaHPO}_4 \cdot 2\text{H}_2\text{O}$  precipitation and deposits on the surface of the substrate and thus forms the coating.

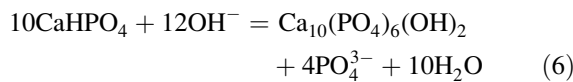


It follows that the electrochemical deposition process includes the ionization reaction, the electrochemical half reaction, the acid base reaction, and the precipitation reaction.

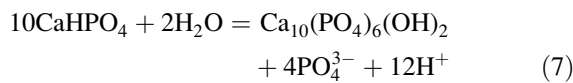
When the hydrothermal treatment is applied to the coated samples, the water in the steam is reduced according to the following equation [18]:



This allows the following reaction to take place:



By combining Equations 5 and 6 the HAp formation reaction can take the following form:



During the hydrothermal treatment, the pH value of the water decreases. However, the pH value must not be allowed to decrease too much, or the reaction will not be maintained. This may explain why the addition of ammonia can increase the formation rate of HAp.

### 3.4. Kinetic analysis of HAp formation

According to the Arrhenius equation, the reaction rate takes the following form:

$$V = \frac{dc}{dt} = KC^n \quad (8)$$

$$K = Ae^{(-E/RT)} \quad (9)$$

Where  $c$  is the HAp content,  $t$  is the reaction time,  $K$  is the rate constant,  $n$  is the reaction order,  $E$  is the

activation energy,  $T$  is the reaction temperature,  $R$  and  $A$  is the constant.

During the reaction time  $t$ ,  $x\%$  of the reagent is converted into HAp, i.e.

$$\frac{dx}{dt} = K'(1-x)^n \quad (10)$$

$$K' = A'e^{-E/RT} \quad (11)$$

the HAp content,  $x$ , can be quantitatively measured using XRD after the samples have been treated for a different duration (Fig. 6).

From Equation 10, Equation 12 can be obtained:

$$\ln\left(\frac{dx}{dt}\right) = n \ln(1-x) + B \quad (12)$$

Using the data in Fig. 6, the linear curve

$$\ln\left(\frac{dx}{dt}\right)$$

versus  $\ln(1-x)$  can be plotted (Fig. 7), and the reaction order,  $n$ , can be deduced from the slope. The results are 2.060, 1.996 and 2.000, respectively, for treatment temperatures of 110, 130 and 150 °C. It follows from the calculation that the reaction may be regarded as a second order reaction ( $n = 2$ ).

Substituting 2 for  $n$  in Equation 10 and carrying out the integration produces the following result:

$$\frac{1}{1-x} = k't + M \quad (13)$$

By plotting  $(1/1-x)$  against  $t$  (Fig. 8),  $K'$  can be obtained from the slope. The results are 0.249, 1.081 and 4.250, respectively, at 110, 130 and 150 °C.

Derived from Equation 11, Equation 14 is obtained:

$$\ln K' = -\frac{E}{RT} + \ln A' \quad (14)$$

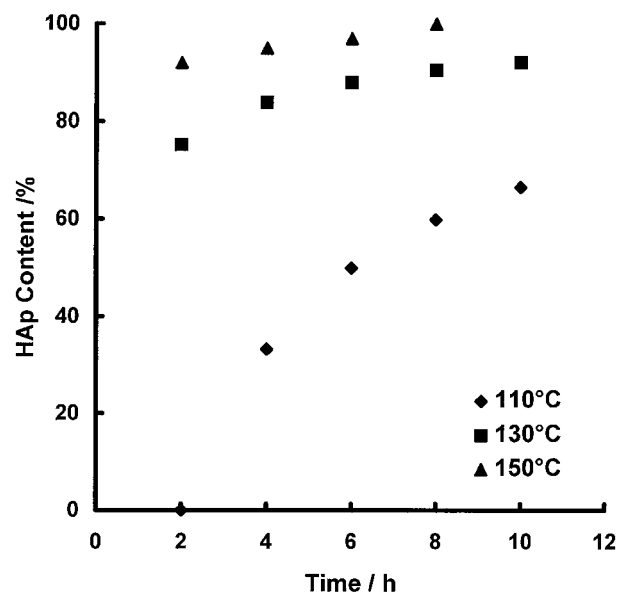


Figure 6 The effects of temperature and time on the HAp content.

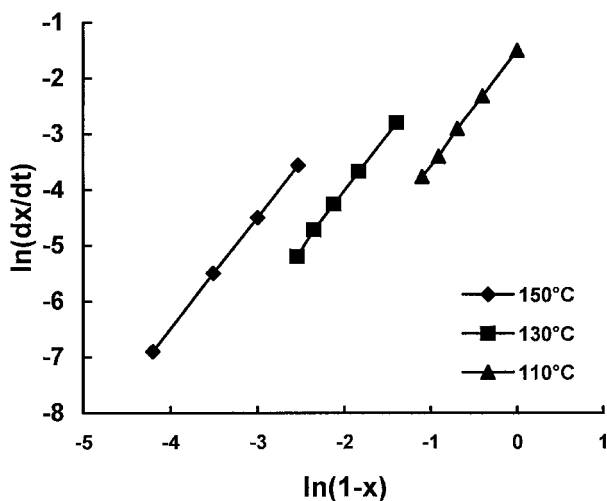


Figure 7 The curves for obtaining reaction order  $n$ .

Since the values of  $(E/R)$  and  $A'$  can be obtained from the  $\ln K'$  versus  $(1/T)$  curve, the apparent activation energy value,  $E$ , and the constant,  $A'$ , can then be calculated. The figures obtained were 94.4 KJ/mol and  $1.81 \times 10^{12}$  respectively.

Ultimately, the Arrhenius relationship for the conversion of  $\text{CaHPO}_4 \cdot 2\text{H}_2\text{O}$  into HAp during hydrothermal treatment becomes:

$$V = A e^{-E/RT} c^2 \quad (15)$$

where  $E$  and  $A$  are 94.4 KJ/mol and  $1.81 \times 10^{12}$  respectively.

#### 4. Conclusion

Pure  $\text{CaHPO}_4 \cdot 2\text{H}_2\text{O}$  coatings on Ti-6Al-4V substrates can be fabricated at relatively low temperatures from aqueous electrolytes containing Ca- and P- bearing ions using an electrochemical deposition process. After hydrothermal treatment,  $\text{CaHPO}_4 \cdot 2\text{H}_2\text{O}$  is converted

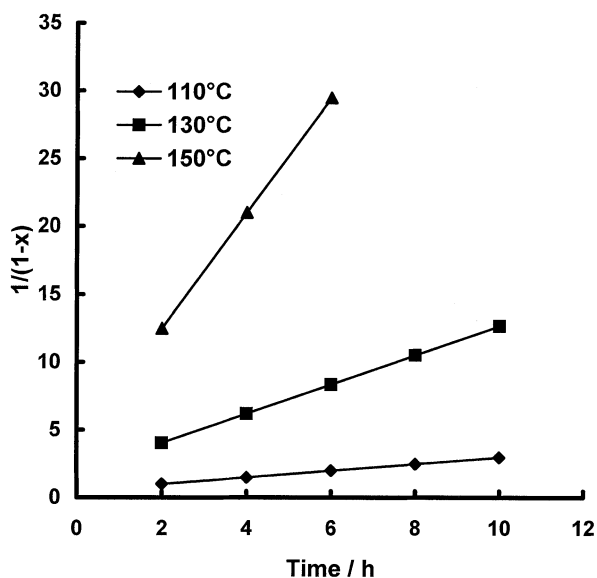


Figure 8 The relationship between  $(1/1-x)$  and  $t$  at different temperatures.

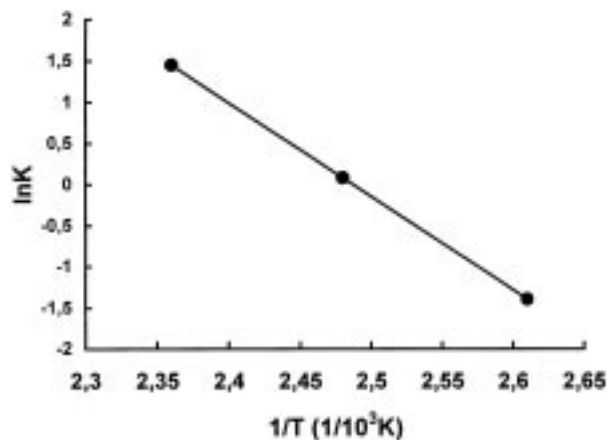


Figure 9 The Arrhenius relationship plot of HAp formation.

into hydroxyapatite. The HAp content of the coatings increases with the treatment temperature and time. As the pH value in the water increases, the hydrothermal reaction rate can be stepped up by the basic steam and affect the crystallographic nature of HAp. HAp coatings have a needle-like microstructure and porous macrostructure, which enhances the growth of the bone tissue.

The synthetic sequence for the formation of  $\text{CaHPO}_4 \cdot 2\text{H}_2\text{O}$  coatings is considered to be a combination of the ionization reaction, electrochemical half reaction, acid base reaction, and precipitation reaction. The function of the hydrothermal treatment is also found to be the synthesis reaction of HAp from  $\text{CaHPO}_4 \cdot 2\text{H}_2\text{O}$ . An Arrhenius relationship linking up the conversion rate and temperature is obtained for the conversion of  $\text{CaHPO}_4 \cdot 2\text{H}_2\text{O}$  into HAp. An apparent activation energy of 94.4 KJ/mol can be obtained by calculation.

#### Acknowledgments

The authors would like to express their thanks to the Sino-France Advanced Research Program (grant number PRA MX-9604) and the Chinese Nature Science Foundation (NSF grant number 59 872 026) for their financial support of the research work reported in this paper.

#### References

1. K. DE GROOT, *Biomaterials* **1** (1980) 47.
2. D. P. RIVERO, J. FOX, A. K. SKIPOR, R. M. URBAN and J. O. GALANTE, *J. Biomed. Mater. Res.* **22** (1988) 191.
3. S. D. COOK, J. F. KEY, K. A. THOMAS, R. C. ANDERSON, M. C. REYNOLD and J. JARCHO, *J. Dent. Res.* **65** (1968) 222.
4. S. J. YANKEE, B. J. PLETKO, H. A. LUCKEY and W. A. JOHNSON in "Thermal Spray Research and Applications", Proceeding of the Third National Thermal Spray Conference, edited by T. F. Bernicki (Long Beach, CA, USA, May 1990) p. 433.
5. C. Y. YANG, *J. Mater. Sci.: Mater. Med.* **6** (1995) 249.
6. A. TISELIUS, S. HLERTEN and O. LEVIN, *Arch. Biochem. Biophys.* **65** (1956) 132.
7. J. REDEPENNING and J. P. MCLSAAC, *Chem. Mater.* **2** (1990) 625.
8. M. SHIRKHAZADEH, *J. Mater. Sci. Lett.* **10** (1991) 1415.
9. *Idem.*, *J. Mater. Sci.: Mater. Med.* **6** (1995) 90.
10. P. DUCHEYNE, S. RADIN, M. HENGHEBAERT and J. C. HENGHEBAERT, *Biomaterials* **11** (1990) 244.

11. G. H. NANCOLLAS and B. TOMAZIC, *J. Phys. Chem.* **78** (1974) 2218.
12. A. S. POSNER, *Clin. Orth. Relat. Res.* **200** (1985) 87.
13. S. D. COOK, J. F. KAY, K. A. THOMAS and M. JARCHO, *J. Oral. Maxillofac. Impl.* **2** (1987) 15.
14. J. M. ZHOU, X. D. ZHANG, J. CHEN, S. ZENG and K. DE GROOT, *J. Mater. Sci.: Mater. Med.* **4** (1993) 83.
15. J. ARENDS, J. CHRISTOFFERSEN, M. R. CHRISTOFFERSEN, H. ECKERT, B. O. FOWLER, C. HEUGHEBAEBAERT, G. H. NANCOLLAS, J. P. YESINOWSKI and S. J. ZOWAKI, *J. Crystal. Growth.* **84** (1987) 515.
16. H. AOKI and K. KATO, *Ceramics Taper* **10** (1975) 7.
17. J. REDEPENNING, T. SCHLESSINGER, S. BURNHAM, L. LIPPIELLO and J. MIYANO, *J. Biomed. Mater. Res.* **30** (1996) 287.
18. E. W. SHI, C. T. XIA, B. G. WANG and W. H. ZHONG, *J. Inorg. Mater.* **11** (1996) 193.

*Received 22 July 1998  
and accepted 17 November 1999*